2022-04-30

Flexible Multiband Multicarrier Signal Design for Broadband Channel Sounding Applications

Asif Iqbal, Micheal Drieberg, Varun Jeoti, Azrina Binti Abd Aziz, Goran Stojanović, Mitar Simić, Nazabat Hussain

Korea Information Processing Society

Asif Iqbal, Micheal Drieberg, Varun Jeoti, Azrina Binti Abd Aziz, Goran Stojanović, et al. 2022. Flexible Multiband Multicarrier Signal Design for Broadband Channel Sounding Applications. Human-centric Computing and Information Sciences 12(19): 1–17. doi: https://doi.org/10.22967/HCIS.2022.12.019.
https://open.uns.ac.rs/handle/123456789/32464

Human-centric Computing and Information Sciences

April 2022 | Volume 12

www.hcisjournal.com

KIPS Korea Information Processing Society

KIPS CSWRG Korea Information Processing Society Computer Software Research Group

HCIS | Human-centric Computing and Information Sciences

RESEARCH (Research Manuscript) Open Access

Human-centric Computing and Information Sciences (2022) 12:19
DOI: https://doi.org/10.22967/HCIS.2022.12.019
Received: December 21, 2021; Accepted: January 27, 2022; Published: April 30, 2022

A Flexible Multiband Multicarrier Signal Design for Broadband Channel Sounding Applications

Asif Iqbal[1,*], Micheal Drieberg[1], Varun Jeoti[2], Azrina Binti Abd Aziz[1], Goran M. Stojanović[2], Mitar Simić[2], and Nazabat Hussain[3]

Abstract

Radio frequency radars have garnered considerable attention in contactless sensing. The congestion in frequency bands and ultra-wideband (UWB) sensing requirements pose challenges to the design of the radars. RF radars can be alternatively considered as channel sounders, which too are facing new channel characterization and modeling challenges owing to new frequency bands in 5th generation (5G) and 6th generation (6G) cellular networks. Various sounding systems were developed to meet the frequency and system bandwidth requirements. However, most offer limited system bandwidth and cannot be easily tuned for different applications. This work aims to address these challenges, by providing a new multiband multicarrier architecture and flexible signal design for channel sounding. Firstly, a channel sounder architecture is developed using commercial software-defined radios (SDRs). Secondly, a new phase-modulated multiband orthogonal frequency division multiplexing (MB-OFDM) waveform, which is designed to provide a flexible frame structure with a low peak-to-average power ratio (PAPR), is proposed to optimize the pulse repetition period for the sounding system by maintaining all the valuable properties of OFDM. The overall system is implemented in a simulated environment, and the results show an improved PAPR performance of the MB-OFDM signal design. In addition, the overall system is tested for different channel conditions and validated against theoretical data. The numerical experiments show that the proposed system is a viable option for UWB channel sounding for a wide range of applications.

Keywords

Radars Sensing, Passive Sensing, Channel Sounder, PAPR, Channel Impulse Response, Channel Characteristics, 5G/6G, OFDM, MB-OFDM

1. Introduction

Radar sensing has already proved its usefulness and significance in defense applications. Recently, radar sensing has been prominently showcased in various domains, such as passive sensing, healthcare, and autonomous vehicles [1, 2]. Contactless sensing of various parameters makes radars an alternative to direct sensing technologies [3]. Lately, transduction-based electromagnetic sensors have been introduced

***Corresponding Author:** Asif Iqbal (asif.iqbal@msn.com)
[1]Department of Electrical and Electronics Engineering, Universiti Teknologi PETRONAS, Perak, Malaysia
[2]Faculty of Technical Sciences, University of Novi Sad, Novi Sad, Serbia
[3]GE Vingmed Ultrasound AS, Horten, Norway

for remote sensing [4–6]. In the same way, the backscattering radar principle is used for passive radio frequency identification (RFID) localization and battery-free surface acoustic wave (SAW) based sensors [7, 8]. The emerging application of battery-free passive sensors is posing new challenges in combating frequency congestion problems. In addition, the demand for new frequency bands is increasing to meet future consumer and industry needs. The envisioned 5G and 6G of cellular networks are focused on enhanced mobile broadband, massive machine-type communication, and ultra-reliable and low latency communications. The 5G network utilizes new frequency spectrums below 60 GHz, while 6G targets to use frequency bands beyond 95 GHz [9, 10], with below 6 GHz having well-understood propagation conditions. However, the propagation behavior of radio waves in new frequency bands needs more study. Generally, each frequency band behaves very differently in a similar propagation environment. Especially in the millimeter wave (mm-Wave) domain, the attenuation factor is very dominant due to oxygen, humidity, and rain. An extensive channel measurement data is required to develop a channel model, and these channel models are then used to design robust modulation schemes for a reliable communication system.

Primarily, radio frequency radar interrogators for passive sensing and channel sounders are similar, and both of them output a channel impulse response (CIR) at the receiver. In brief, sounding the channel with radio signals, acquiring knowledge of propagation phenomenon in specific channels, extraction of model parameters from measurement data, and channel model development are a few of the main objectives of channel sounding. The developed channel models are then used to design and test reliable communication systems. In comparison, radar sensing must similarly first learn the channel characteristics, thus it can accurately decipher the sensing variable by eliminating the effects of the channel. In this work, a more flexible channel sounder design framework is proposed to support various applications.

Sliding correlation is a well-known time domain technique for wideband CIR measurements [11–15]. Various dedicated sliding correlator sounders were proposed to meet the needs for wideband channel measurements [16–20]. Generally, the sliding correlator sounding system transmits pseudo-random noise (PN) sequences and performs a correlation at the receiver with a slightly slower rate identical copy of the PN sequence. Due to the efficient correlation properties of PN, this system can achieve high processing gain, better dynamic range, and fine resolutions [13, 15, 21, 22]. Sliding correlator sounders also have the advantages of low peak-to-average power ratio (PAPR) and efficient data compression for real-time recording. However, this system requires a complex and dedicated hardware system, and the choice of parameters, such as PN sequence length and chip rate, are also critical to optimize this system's performance.

Frequency sweep is another well-known technique among channel sounding techniques. A frequency swept system utilizes a vector network analyzer (VNA) to perform channel sounding [23–26]. The VNA sweeps a set of discrete frequencies within the required bandwidth, and a complex channel frequency transfer function or *S*-parameter S_{21} is then recorded in the acquisition systems. Afterward, inverse discrete Fourier transform (IDFT) is performed to compute the CIR. While straightforward, there are a few practical limitations of the VNA-based sounding system. Firstly, the system is only suitable for a static environment because of its long sweep time. Secondly, the transmitter and receiver must be co-located due to cable length limitations.

To mitigate the limitations of sliding correlation and VNA-based sounders, multicarrier or orthogonal frequency division multiplexing (OFDM)-based sounding systems are developed to perform frequency domain channel sounding [27–35]. In the OFDM sounding system, the probing signal is synthesized in the frequency domain, while IDFT is performed before transmitting into the air. At the receiver, the matched filter operation is performed in digital baseband processors. However, the major problem of multicarrier channel sounder is the high PAPR. In this regard, various sequences have been proposed to reduce the PAPR. OFDM systems are usually implemented on software-defined radio (SDR). Accordingly, simple hardware implementation and faster computation make this technique a strong candidate for channel sounding.

The time resolution of the channel sounder depends on the system's bandwidth. As a result, custom hardware is required for larger instantaneous bandwidth systems, and the overall solution is usually not affordable for many institutes and organizations. Recently, inspired by a VNA, new multiband sweep techniques have been proposed to perform faster and wider bandwidth channel sounding using low-cost commercial off-the-shelf (COTS) equipment. In [36], the authors have proposed a 60-GHz PN sequence-based wideband channel sounder using a heterodyne transmitter and receiver based on an arbitrary waveform generator (AWG), digitizers, and data storage device. To increase the system bandwidth, ten sequential measurements are performed with a 500-MHz frequency step to cover the full 5 GHz. After calibration, the channel transfer function (CTF) of all sub-bands are concatenated in the frequency domain, and IDFT is used to obtain the CIR of the complete 5 GHz channel bandwidth. This system has the advantage of constant envelope (CE) transmission. However, this system can only be used for indoor channel measurements. Bas et al. [37] have proposed another multiband sounding technique based on direct up/down conversion transceivers using AWG, an in-phase and quadrature (IQ) mixer, digitizer, frequency synthesizer, and high-speed data recorder of a redundant array of independent disks (RAID) storage. This system has an instantaneous bandwidth of 1 GHz, and operates from 3 GHz to 18 GHz. A fast-switching system is used to sweep the complete 15 GHz with overlapping frequency sub-bands. The proposed configuration of the system has a maximum delay spread of 2 μs, which limits it to urban and outdoor measurement scenarios, and the overall solution is also not very cost-effective. In [38], the authors have proposed a similar technique to develop a multiband multitone channel sounder. The proposed system is based on low-cost SDR and an open-source software named GNU radio [39]. The SDR can be tuned from a 300 MHz to 3.8 GHz RF frequency range with a maximum of 28 MHz instantaneous bandwidth. Channel sounding is performed in multiple sub-bands, and in each sub-band, 8 multitone are transmitted with phase randomization to reduce PAPR. Due to the latency between PC and SDR communication, this system is only used for the static environment. Li et al. [40] have proposed a frequency domain technique using a multiband (MB) OFDM signal. This sounder is based on superheterodyne SDR with 20 MHz instantaneous bandwidth, and measures 10 continuous sub-bands to cover 200 MHz in 3 ms, while a guard time is used to handle the switching time of hardware. A shared global positioning system (GPS) reference clock is used to synchronize a transmitter (TX) and receiver (RX). This system uses the IEEE Standard 802.11, a frame structure for sounding purposes that consists of the training sequence and data sections. The training section is used for frame and symbol synchronization. Although this system is very cost-effective in terms of hardware implementation, this system uses a shared clock between TX and RX, limiting it to perform channel sounding in an indoor environment. This system also has an inherent problem of the OFDM system, namely poor dynamic range and PAPR. Recently, in [41], the authors have proposed a flexible SDR-based multiband sounder for real-time channel measurement. In their work, a standard OFDM waveform is used as a probing signal. However, the PAPR problem is not addressed for optimal OFDM sounding.

Based on the limitations of the previous MB system, this work has contributed to defining an improved and flexible MB-OFDM-sounding architecture based on COTS SDRs. Particularly, due to the fact that most hardware systems are not suitable for UWB signal, MB-OFDM allows for combining one narrowband hardware into time-interleaved narrowband hardware that mimics MB UWB hardware. OFDM provides a flexible digital implementation of the UWB signal waveform. Nevertheless, the major problem in MB-OFDM signal design is the high PAPR. CE OFDM waveforms are highly encouraged to optimize transmitter performance. In this regard, various techniques have been proposed to reduce PAPR in the OFDM system [42]. Based on the previous limitations, there is a need to design an optimum MB-OFDM signal design. Accordingly, it is hypothesized that the constant amplitude zero autocorrelation (CAZAC) family sequence can provide a low PAPR MB-OFDM spectrum constraint waveform. A new Chu phasing scheme has been introduced in this work to produce a low PAPR probing signal, and an MB-OFDM signal design is developed for channel sounding. In addition, flexible sounding architecture is developed to perform sounding in different environmental conditions.

In order to develop a new OFDM sounding system, a brief introduction to the overall system architecture is needed. Accordingly, Section 2 first introduces a general architecture of an MB-OFDM sounding system. Afterward, in Section 3, a detailed formulation and numerical implementation of the MB-OFDM signal design is presented, and the probing signal is shown to meet all design requirements. Section 4 provides a brief formulation for CIR estimation. In Section 5, a discussion on the procedure to evaluate the methods' performance and its validation against those in the literature is presented. A conclusion of the study is presented in Section 6.

2. Proposed Multiband Sounder Design

Conventionally, the hardware of radios is implemented on a component level, and most of the functionality is achieved using analog circuitry, while a fixed hardware platform limits the use of radios to a few specific applications. On the other hand, the SDR approach provides a versatile platform for re-programmable applications, and divides the radio functionality into two parts, a programmable digital platform and wideband analog frontend. The digital platform of SDR is built using a digital processor (DP) and field-programmable gate array (FPGA). The analog front is designed for a wide range of tunable RF frequencies, so that this makes SDR a highly desirable tool for R&D and implementation of new communication systems. This architecture also offers another advantage of using high-level programming languages for faster prototyping.

Given the hardware specification of SDRs, it is noted that almost all COTS SDRs offer only a few MHz of baseband signal bandwidth. Due to limited signal bandwidth, the available SDR systems cannot perform UWB channel sounding for finer time resolution. In this work, a multiband approach has been adapted for UWB communication making use of the IEEE 802.15.3a standard [43]. However, the proposed multiband sounder approach is different in several aspects (e.g. the signal bandwidth for the channel sounder is not fixed). Similarly, the physical layer is highly flexible to meet the sounding requirements.

2.1 Multiband OFDM Probing Signal Design Concept

In a multiband-sounding approach, various narrow bandwidth sub-bands are concatenated together to form a UWB frequency band. Each sub-band occupies a signal bandwidth per hardware specifications. In this regard, this approach offers the advantage of utilizing the standard SDR for UWB sounding, and the use of OFDM modulation provides spectral flexibility and control over the transmit power. In addition, the processing requirement is also very small since a much smaller bandwidth needs to be processed at one time.

Consider a UWB system built by concatenating S sub-bands as shown in Fig. 1. Each sub-band occupies a baseband signal bandwidth (BW), where the signal BW is defined by SDR hardware specifications. Each sub-band is further divided into N orthogonal subcarriers. An OFDM symbol in the time domain, $x(n)$, is constructed using inverse fast Fourier transform (IFFT) of complex numbers corresponding desired pilots at the N frequency bins. The resulting time domain samples of OFDM symbol, $x_m(n)$, for m^{th} period can be written as [44],

$$x_m(n) = \sum_{k=0}^{N-1} s_m(k) \exp(j2\pi nk/N), \tag{1}$$

where $s_m(k)$ represents a complex modulated symbol to be transmitted in subcarrier k. The frequency spacing between adjacent subcarriers is $\Delta f = BW/N$. The resulting time-domain waveform has a duration of $T_b = 1/\Delta f$. Let T_c be the duration of a cyclic prefix, which is created by copying the last N_c samples of IFFT and concatenating them to the front of the symbol. This gives a continuous waveform

where the symbol and cyclic prefix are joined together to provide sufficient time for the longest significant path of the CIR. A guard time, T_g is also added at the end of the symbol to prevent a windowing effect from attenuating the sample within T_b period. It can also be used to cater to the switching time between carrier frequencies. Thus, the total duration of an individual OFDM symbol is

$$T_{sym} = T_b + T_c + T_g. \tag{2}$$

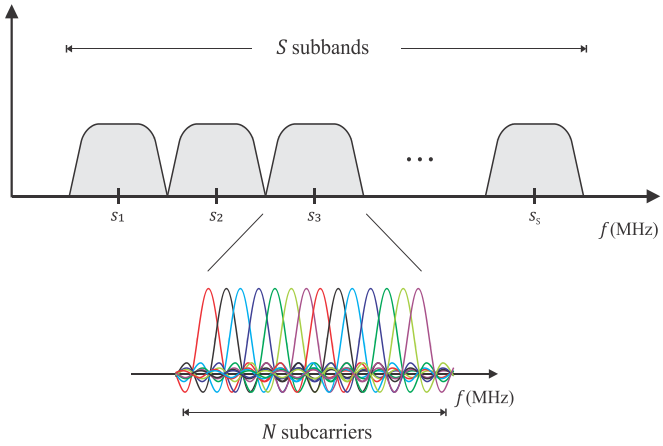

Fig. 1. UWB multiband OFDM spectrum.

The coherence time & bandwidth of the channel define the requirement for the maximum T_{sym}. It is carefully crucial to select the symbol length according to the channel condition. Since the switching time between carrier frequencies T_g depends on the hardware specification and is usually expressed in nanoseconds, T_b and T_c are used to control the overall symbol duration.

As described before, the UWB band is divided into S sub-bands, with the center frequency f_c for each sub-band with baseband BW calculated with the equation shown below:

$$f_c = f_o + \text{BW} \times s, \tag{3}$$

where f_o is the center frequency for first sub-band and $s = 1,2, \ldots, S$.

In a multiband sounder, channelization is based on time-frequency codes and the number of transmitting streams, which is considered as different users. Each user has a unique code, each of which defines the center frequency of allocated sub-bands to one user and is generated for each user to cover the full bandwidth in the shortest possible time. Ideally, a larger separation of the band for each time window is advisable. However, for sounding application, the minimum separation kept is one, and there is no collision between multiple transmit streams. For example, for only one transmit stream, the code generated has a length of $s = 1,2, \ldots, S$. However, if we have two transmit streams, the code length will become half of s, and the subsets will not have common bands. Let us consider the same example given above where $S = 6$. If a hardware resource has only one transmitter, the code generated is $\{1,2,3,4,5,6\}$. However, if two transmitters are available, the code for the first transmitter can be $\{1,3,5\}$ while the second transmitter will have a code of $\{2,4,6\}$. Fig. 2(a) and 2(b) illustrate the time-frequency code for one transmit stream and two transmit streams, respectively. For sounding applications, the code can also be shuffled as long as it covers a whole sounding frequency band. In other words, the proposed multiband sounding system has a similarity to VNA, where a single carrier is swept through a required frequency band. In the proposed method, the wideband signal is swept to provide a frequency response of UWB. Another advantage of this technique is that the sounding can also be performed in a cognitive model to avoid any interference between sounding and existing users.

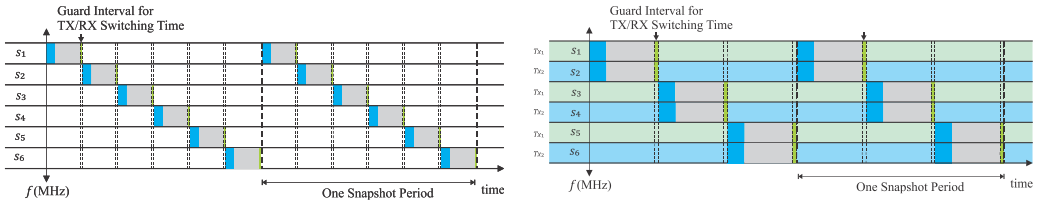

(a) (b)

Fig. 2. Time-frequency representation of a multi-band OFDM signal: (a) one transmitter code $\{1,2,3,4,5,6\}$ and (b) two transmitters code $Tx_1 = \{1,3,5\}$ and $Tx_2 = \{2,4,6\}$.

The multiband OFDM sounder uses standard OFDM block sets to build a physical layer as shown in Fig. 3. Since the focus of this work is to evaluate the performance of multiband OFDM soundings signal design and channel estimation block set, it is also assumed that the transmitter and receiver are perfectly synchronized. The block sets, such as a scrambler & de-scrambler, convolutional encoder & Viterbi decoder, and bit interleaver & de-interleaver, as well as synchronization are not discussed in this work. The reader may find additional information about these block sets in [44].

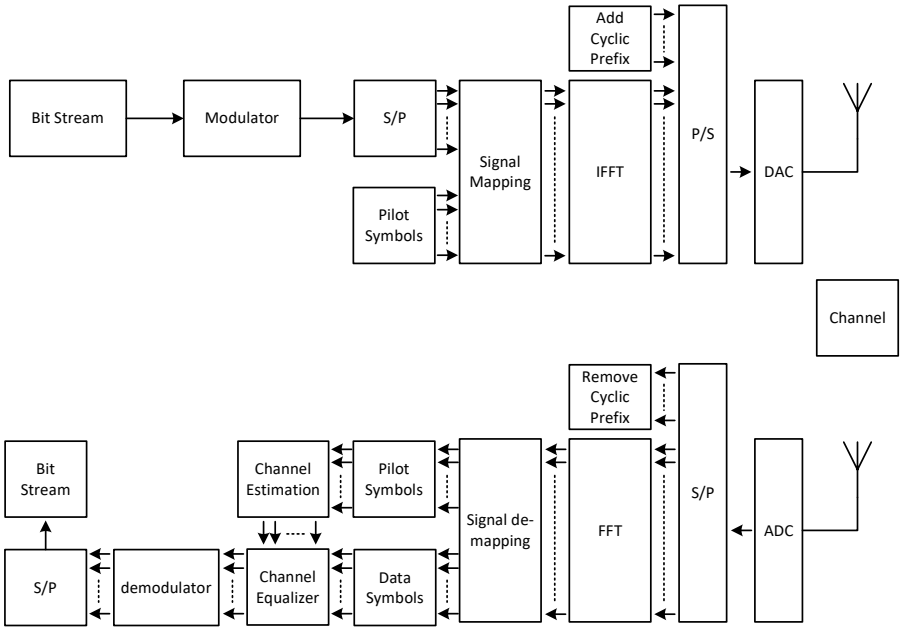

Fig. 3. OFDM system transmitter and receiver architecture.

2.2 OFDM Subcarrier Frequency Allocation

In the OFDM sounding system, the fundamental sampling of discrete tones is defined by the FFT size N. Among N subcarriers, N_d data tones are used for data transmission, and N_p pilot tones are used for training. The number of guard subcarriers at the lower band edge is N_{gl}, and the number of guard subcarriers at the upper band edge is N_{gu}. In total, $N_g = N_{gl} + N_{gu}$ are kept as guard subcarriers. The DC sub-carrier, $N_{dc} = \frac{N}{2} + 1$, is not available to avoid error build-up at DC due to receiver imperfections. The number of useable carriers, N_u for link signaling and carrying payload data are as follows:

$$N_u = N_d + N_p - 1, \qquad \text{where } N_u < N - N_g \tag{4}$$

For sounding mode, $N_d = 0$ and $N_p = N - N_g - 1$. The pilot tones q_{k_p} for m^{th} symbol are assigned from a complex-valued p_u sequence expressed as:

$$q_{m,k_p} = p_{m,u}, \tag{5}$$

where, $k_p = N_{gl} + 1, N_{gl} + 2, \dots, N_{gl} + \frac{N}{2}$, $N_{gl} + \frac{N}{2} + 2, \dots, N_{gl} + N_p$, $m = 0,1,2, \dots, M_{sym} - 1$, $u = 0,1,2, \dots, N_p - 1$, and M_{sym} is the M^{th} symbol. In (5), p_u is either BPSK or polyphase modulated sequence. The guard subcarriers $g_{m,k}$ takes the location expressed as:

$$g_{m,k_g} = 0, \tag{6}$$

where $k_g = 1,2,3, \dots N_{gl}$, $N_{gl} + N_p + 1, N_{gl} + N_p + 2, N$.

For a hybrid mode, the complex data symbols, d is grouped in N_d size. For m^{th} symbol, d is the assigned to carriers c_{k_d} expressed as:

$$c_{m,k_d} = d_{u_d + N_d m}, \tag{7}$$

where, $u_d = 0,1,2, \dots, N_d - 1$, $m = 0,1,2, \dots, M_{sym} - 1$, and k_d indexes are computed as follows:

Let $A_{sub} = \{1,2,3, \dots, N\}$, is a set which contains all available frequency bin indices and B_g is a subset of A_{sub} for guard subcarriers indices, $B_g = \{1,2,3, \dots N_{gl}, N - N_{gu} + 1, N - N_{gu} + 2, N\}$. The DC sub-carrier element is $B_{dc} = \left\{\frac{N}{2} + 1\right\}$. The useable subcarrier subset can be written as,

$$A_u = A_{sub} \backslash (B_g \cup B_{dc}) = \{N_{gl} + 1, \dots, N/2, N/2 + 2, \dots, N - N_{gu}\}. \tag{8}$$

If the OFDM symbol contains no pilot tones then $k_d \subseteq A_u$, otherwise $k_d \subset A_u$ and the number of elements of k_d is equal to N_d. The pilot tones q_{m,k_p} for mth symbol are assigned from a complex-valued, p_{u_p}, sequence as,

$$q_{m,k_p} = p_{m,u_p}, \tag{9}$$

where $k_p = A_u \backslash k_d$, $u_p = 0,1,2, \dots, N_p - 1$ and $m = 0,1,2, \dots, M_{sym} - 1$.

Fig. 4 shows the hybrid mode subcarrier frequency allocation for 64-FFT size case. In this example, 10 guard carriers, 4 data carriers, and 49 pilots are used.

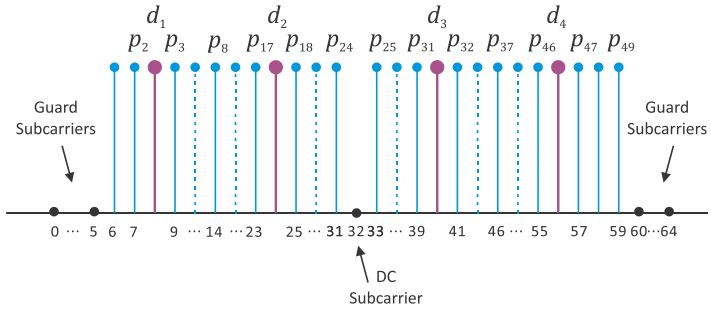

Fig. 4. Subcarrier frequency allocation for hybrid mode.

2.3 Sounding Subframes Structure

A frame-based transmission is used in the proposed multiband sounder. The OFDM symbols are concatenated to form subframes. A frame comprises two major components, a training sequence and a data section, as shown in Fig. 5. The primary objective of the training sequence is synchronization and the retrieval of a coherent data sample. A data section consists of multiple OFDM-sounding symbols. Suppose the cyclic prefix is set to zero. In that case, a minimum of three identical OFDM sounding symbols are required for an unambiguous CIR estimation, and CIR length will be equal to the duration of the symbol. However, if the cyclic prefix length is set to the fraction of the OFDM symbol length, the minimum number of symbols required is only one. Ideally, more than 2 data symbols are transmitted to provide better estimation performance. The number of data symbols, N_{sym}^{data} and the number of training symbol, $N_{sym}^{training}$ are set to be flexible for sounder because it highly depends on the channel properties. The duration of the subframe containing $N_{sym}^{sub} = N_{sym}^{training} + N_{sym}^{data}$ symbols are:

$$T_{subframe} = N_{sym}^{sub} \times T_{sym}. \tag{10}$$

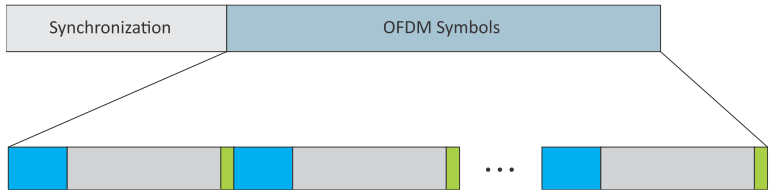

Fig. 5. Frame structure of OFDM sounding.

3. OFDM Pilot Sequence Design for Low PAPR

In a communication system, the preamble-sounding symbols are constructed in time-domain using CAZAC sequences. A CAZAC sequence provides constant envelope properties. However, it limits the use of symbols to only sounding, and no data can be transmitted during that time.

In this work, the sounding scheme is developed to provide flexibility for simultaneous sounding and data transmission. Although the data transmission is not a primary objective of a sounder, there are cases where TX and RX are not co-located, and there may be a need to exchange data between TX and RX. Hence, the proposed system has different challenges to meet the MB-OFDM sounding system requirement, and it has more similarities to OFDM data symbols where symbols are constructed in frequency-domain for better flexibility and control over data pilot subcarriers and spectrum shaping.

3.1 Phase Sequence for Pilot Tones

Let $s_m(k) = c_m(k) + q_m(k)$, in (1), where $c_m(k)$ and $q_m(k)$ are complex-valued data and pilots tones transmitted in the k^{th} subcarriers, respectively. Using (1), the time-domain samples of m^{th} OFDM can be rewritten as,

$$x_m(n) = \sum_{k=0}^{N-1} [c_m(k) + q_m(k)] \exp(j2\pi nk/N). \tag{11}$$

The crest factor of $x_m(n)$ is a critical parameter to optimize the PA performance. Multicarrier techniques are prone to the high PAPR because the phase of tones is dependent on the constellation of a random input data stream and pilot sequence. The instantaneous power can be written as,

$$P(n) = |x(n)|^2. \tag{12}$$

The average power is given by,

$$P_{avg}(n) = \text{avg}\{|x(n)|^2\}, \tag{13}$$

and PAPR is the ratio of maximum envelope power to average power. Thus,

$$PAPR = \frac{\max\{P(n)\}}{P_{avg}(n)}. \tag{14}$$

The data tones, $c_m(k)$, are assigned from the QPSK or QAM constellations, whereas pilot tones, $q_m(k)$, are unity-gain phase-modulated tones that take values from sequences $p_m(u)$ as described below,

$$p_m(u) = a_m(u)\exp j(\theta_m(u)). \tag{15}$$

Here, $a_m(u)$ and $\theta_m(u)$ are amplitude and phase associated with u^{th} element of sequence for m^{th} symbol, and $j = \sqrt{-1}$ is an imaginary number. The crest factor of $x_m(n)$ caused by pilot sequence is dependent on the phase angle $\theta_m(u)$. Each element of the pilot sequence $p_m(u)$ is assigned to dedicated tones in the frequency domain using (9). The choice of phase angle is very critical to the PAPR of the transmit signal. Having the same phase for all tones is the worst choice. Conventionally, pilot subcarriers are BPSK modulated with pseudo-random binary sequence (PRBS). PRBS is generated using linear feedback shift registers (LFSR). Though this is better than the same-phase case, the PAPR still grows as the number of tones increases. In [45], the author used PRBS sequence-based phase randomization with a recursive algorithm to reduce the PAPR. However, these recursive algorithms require very high computational effort, especially for a large number of carriers. On the other hand, there is another approach where researchers look for sequences that can provide a phasing scheme that achieves the desired low PAPR waveform without the need for recursive algorithms, precoding, or clipping methods [46].

In this work, a new phasing scheme based on the Zadaff-Chu (ZC) sequence is used [47]. In the proposed method, symbols are synthesized in the frequency domain, and phase randomization of pilot tones is performed using the phases from the ZC sequence. A ZC sequence is given by

$$p_m^{Chu}(u) = a_m^{Chu}(u)\exp(\theta_m^{Chu}(u)). \tag{16}$$

In (16), a_m^{Chu} is the amplitude of sequence and θ_m^{Chu} is the phase, described as

$$\theta_m^{Chu}(u) = -j\frac{\pi\gamma u(u + c_f + 2\kappa)}{N_p}, \tag{17}$$

where, $0 \le u < N_p$, $0 < u < N_p$ and $\gcd(N_p, \gamma) = 1$, $c_f = N_p \bmod 2$, $\kappa \in \mathbb{Z}$, N_p = length of the sequence.

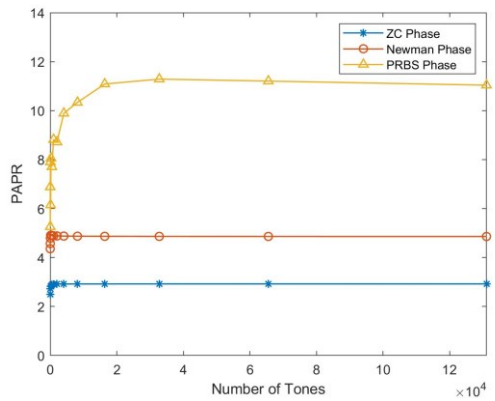

Fig. 6. Comparison of PAPR for ZC, Newman, and PRBS phase.

The sounding pulse duration depends on the channel conditions, while frequency-selective channels may require a very large FFT size. Thus, the pilot sequence must have a low PAPR for large numbers of pilot tones. As a result, a detailed comparison of 64 up to 130k number of tones is presented in Fig. 6 for PRBS, Newman, and ZC phasing schemes. It can be observed that the ZC phasing scheme gives the lowest PAPR for a sufficiently large number of tones.

3.2 Sounding Signal PAPR in the Presence of Data Tones

In the previous section, it has been shown that the proposed ZC sequence-based phase randomization of pilot tones provides an optimum PAPR performance. However, for hybrid or data transmission cases, where data subcarriers are assigned from a complex-valued constellation, additional PAPR results, for which Monte Carlo simulations are performed to provide a complementary cumulative distribution function (CCDF) of PAPR in the presence of data tones for data transmission cases.

The results provide a comparison of different FFT sizes, and the 4-QAM modulation is used for all cases, with system BW being kept constant at 20 MHz. An example of OFDM subcarrier mapping for 64-FFT size for data transmission cases is illustrated in Fig. 7(a), in which the y-axis represents the frequency bin, and the x-axis the number of symbols. The OFDM subcarrier mapping remained the same for all symbols. The color map is used to depict different types of subcarriers. The number of data subcarriers is approximately 50% of useable subcarriers for each FFT size case. Fig. 7(b) presents the PAPR for different sizes of FFT length, and the results are also compared with PRBS for 16-FFT size. For the data transmission case, the PAPR contribution of the data carrier is very dominant, and a larger FFT size has a PAPR close to 11 dB. A comparison between PRSB and ZC-based pilots is presented for the PRSB 16k-FFT size. Accordingly, it can be observed that the PRSB case has around 12.5 dB PAPR, and the ZC based scheme performs better than PRSB for similar system configurations, so that it can be concluded that the PAPR with the ZC pilot sequence is between 9 to 11 dB.

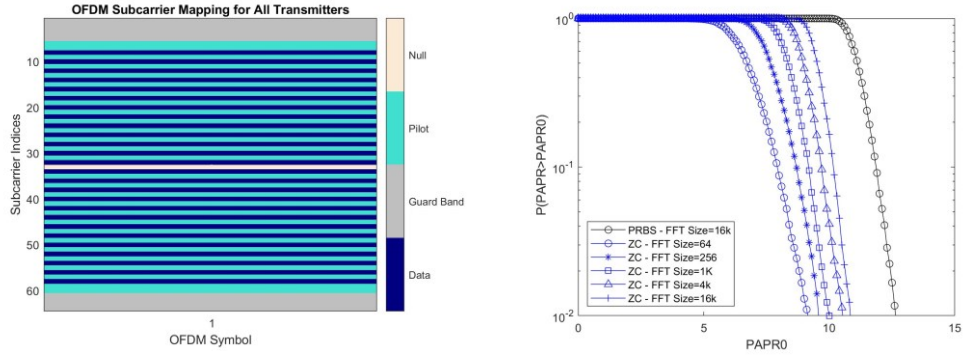

(a) (b)

Fig. 7. (a) OFDM subcarrier mapping for data transmission mode. (b) PAPR comparison of different length ZC sequences and 16K PRBS for hybrid mode.

In the above examples, PAPR reduction techniques, e.g., precoding matrices clipping [46], are not used to provide a comparison of worst-case scenarios. If we employ PAPR reduction techniques for data subcarriers, the data transmission PAPR can be further reduced. Hybrid sounding systems, where data and probing signals are transmitted together, may be needed in radar sensing applications. The proposed phasing provides a superior performance compared to the conventional method in data transmission mode. Thus, it can be concluded that the designed probing signal provides the flexibility of configuration and meets the requirement for the sounding waveform of a low PAPR.

4. Channel Impulse Response Estimation

The impulse response of the multipath channel for an ideal Dirac pulse, $\delta(n)$, can be given from the equation:

$$h(n) = \sum_{l=0}^{L-1} \alpha_l e^{j\theta_l} \delta(n - \tau_l), = \sum_{l=0}^{L-1} h_l \delta(n - \tau_l), \tag{18}$$

where L is the total number of multipath, α_l is the amplitude, τ_l is an additional time delay and $\theta_l = 2\pi f_c \tau_l$ is the phase associated with the l^{th} path. The transmitted signal, $x_m(n)$, goes through the multipath channel and a received baseband signal, $y_m(n)$, for m^{th} symbol can be written as:

$$\begin{gathered} y_m(n) = \sum_{l=0}^{L-1} h_{m,l} x_m(n - \tau_l) + w_m(n), \quad \text{or} \\ y_m(n) = h_m(n) * x_m(n) + w_m(n), \end{gathered} \tag{19}$$

where $w(n)$ is additive white Gaussian noise (AWGN). As the cyclic prefix OFDM system is related to periodic convolution between the channel and OFDM symbols, (19) can be written as:

$$y_m(n) = h_m(n) \circledast x_m(n) + w_m(n), \tag{20}$$

where operator $\circledast$ represents periodic convolution.

CIR, $h_m(n)$, estimation is a challenge in a time-varying environment. Generally, blind, non-blind, and semi-blind estimation techniques are used for channel estimation. However, non-blind methods perform better because known information is available at the receiver for the estimation of CIR, while in non-blind schemes, pilots are commonly used. In this regard, different types of pilot arrangement, block, comb, and lattice, are proposed to optimize the pilot density and system performance in several kinds of channels [48]. The least-square (LS) and minimum mean-square error (MMSE) channel estimation techniques are well known for the pilot-assisted OFDM system, and while the LS technique is computationally efficient, it however suffers from poor accuracy. On the other hand, MMSE requires very high computation but provides better accuracy [48, 49]. Recently, time-domain correlation-based techniques such as frequency-domain pilots & time-domain correlation (FPTC) have been introduced to improve computational efficiency [50–52].

Since, the objective of this work is to develop the signal design, conventional channel estimation techniques are used for performance measurement.

5. Results & Discussion

Extensive numerical experiments are performed to extend the validation of the proposed multiband channel sounders, and the proposed channel sounder is implemented in MATLAB. In this work, known CSI is used as a benchmark, and conventional techniques are also implemented such as LS, DFT-based LS, and FPTC in a similar MATLAB environment to evaluate the proposed sounder. The testing is performed to show that the particular implementation of the proposed CIR estimation techniques is valid and suitable for its intended purpose, respectively, within a reasonable bound of accuracy. For a detailed performance evaluation, mean-square error (MSE) is computed for each case with known CIR as a reference. The channel transfer function (CTF) is computed using FFT of CIR, with the formula used to calculate MSE given by [53]:

$$MSE = E\left\{\left|H(k) - \widetilde{H}(k)\right|^2\right\}, \tag{21}$$

where $H(k)$ is the known CTF and $\widetilde{H}(k)$ is the estimated CTF using proposed and conventional

techniques. An average MSE is computed based on a Monte Carlo simulation for different SNR scenarios in various environmental conditions.

It is assumed that two coherent and independent transmitter resources are available—each transmitter supports a 20 MHz of the system bandwidth. In addition, a multiband bandwidth of 200 MHz is considered, and the total number of sub-bands is 10. As described in the previous section, a unique time-frequency code is used for each transmitter. Transmitter one has assigned code $\{1,3,5,7,9\}$, and transmitter two the code $\{2,4,6,8,10\}$. A resource mapping of multiband switching is shown in Fig. 8. Since we have two transmitter resources available, there are a total number of five switching time slots and switching between two bands has a guard duration. Here, the system configurations of the spectrum constraint hybrid mode are used for the simulation. The FFT length of 64-point is used for each sub-band, and a cyclic prefix of ½ of FFT-size is used. The symbol duration without cyclic prefix and guard period is 3.2 μs. The 4-QAM data modulation order is used, and the MSE results are compared with those from theoretical and conventional techniques, with the summary of simulation parameters given in Table 1.

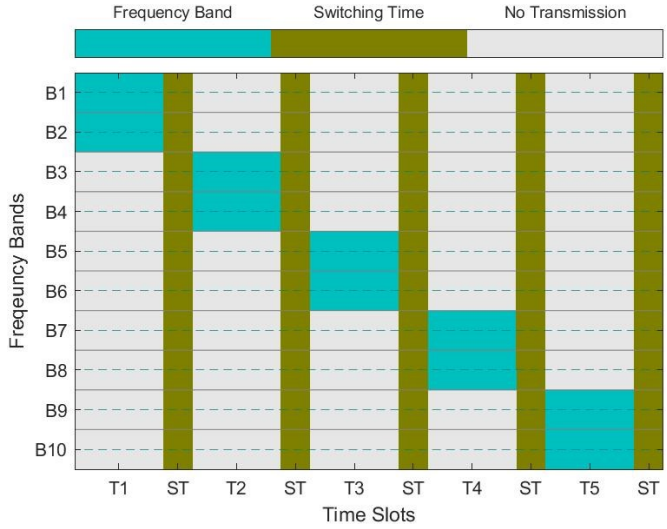

Fig. 8. Resource mapping of multiband OFDM sounder.

Table 1. Simulation parameters for multiband transmission in Rayleigh channel

System parameter	Value
Data transmission mode	
Number of pilot subcarriers	27
Number of data subcarriers	26
QAM order	4
Number of guard subcarriers	10
Δf: subcarrier spacing (kHz)	312.5
T_b: OFDM Symbol duration of sub-band (μs)	3.2
T_c: Cyclic Prefix duration of sub-band (μs)	1.6
T_g: Guard Interval duration (μs)	0.25
T_{sym}: Symbol duration (μs)	5.05
Number of sub-bands	10
Number of transmitters	2

To evaluate the performance of the proposed sounder, a more challenging frequency selective Rayleigh channel is used. The power delay profile of the 6-tap channel is described in Table 2, and Fig. 9(a) shows the semi-logarithmic plot of MSE results from the Monte Carlo simulations for Eb/No values ranging

from 0 until 30 dB. The results compare LS, LS-DFT, and FPTC at different iteration levels, and from the results, it is observed that LS and FPTC have similar performance. However, LS-DFT performed better than LS and FPTC for the frequency selective channel. In other words, for a fixed threshold of MSE at 10^{-3}, LS and FPTC require 17 dB of Eb/No while LS-DFT can reach the threshold of performance at 15 dB, which is better against other techniques. In addition, it can also be observed that LS-DFT performs better for less than 15 dB Eb/No. However for higher Eb/No, there is no significant advantage of using LS-DFT due to the additional computation burden it brings for FFT operations.

Table 2. Power delay profile for a frequency selective Rayleigh channel

Path No.	Delay (μs)	Power (dB)
1	0	-3
2	0.0020	-9
3	0.0100	-3
4	0.0500	-6
5	0.2000	-9
6	0.3000	-12

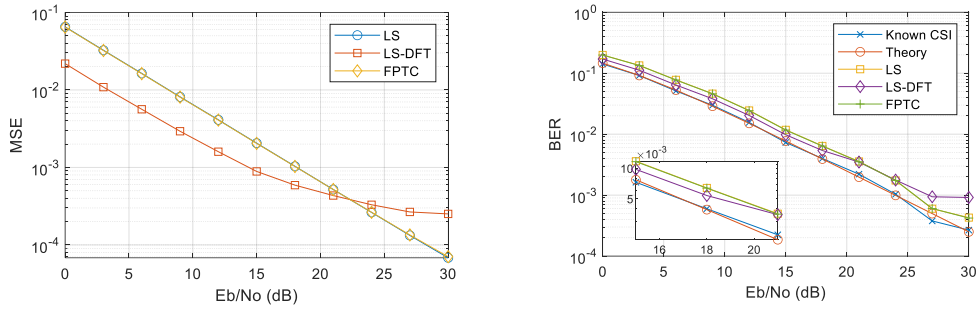

(a) (b)

Fig. 9. (a) Comparison of MSE performance for conventional techniques in a frequency-selective Rayleigh channel. (b) Comparison of BER performance for conventional techniques in a frequency-selective Rayleigh channel.

As explained in the experiment setup above, a data transmission or hybrid system configuration is used to evaluate the sounders' performance. Since data is also transmitted on approximately 50% of available subcarriers, Fig. 9(b) shows the comparison of BER results from LS, LS-DFT, and FPTC. A zoomed-in plot of BER for 15 to 21 dB of Eb/No is also provided for a detailed comparison and insight. As we have discussed, the MSE of LS-DFT only performs better for lower Eb/No values, and it is also apparent from the results that BER is higher for LS-DFT as compared to other techniques for high Eb/No values.

For further study, a comparison of an instantaneous CIR from simulations is presented for a 30 dB Eb/No in Fig. 10(a). The x-axis represents the time from 0 to 1.2 μs and y-axis represent the amplitude of each channel tap. As described in the simulation setup, we have assumed six tap Rayleigh channels to evaluate the proposed sounder's performance. It can be observed from results that the proposed multiband can clearly identify a high-resolution impulse response. The CTF of Fig. 9(a) is computed to provide detailed insight, and a comparison of an instantaneous CTF between conventional techniques is presented for 30 dB Eb/No in Fig. 10(b). The x-axis represents the 40 MHz frequency channel, while the y-axis provides channel gain in dB. The CTF of the known CSI case does not include the noise artifact. However, theoretical results are computed with AWGN noise. Each sub-channel is 20 MHz wide and has spectrum constraints due to a guard band and DC subcarrier. For LS, the interpolation error can be seen at the edge of the sub-channels. Accordingly, to provide better visualization, the CTF of known CSI is compared with other techniques and 40 MHz around a DC carrier, which is illustrated in Fig. 10(b). From

the results, it can be concluded that the proposed multiband sounder is suitable for higher resolution impulse response measurements.

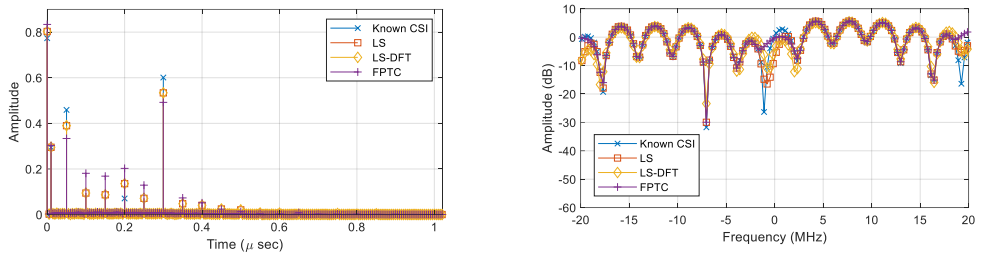

(a) (b)

Fig. 10. (a) Comparison of CIR performance for conventional techniques in a frequency-selective Rayleigh channel. (b) Comparison of CFR performance for conventional techniques in a frequency-selective Rayleigh channel.

6. Conclusion

In this work, a detailed design methodology of a flexible multiband OFDM sounding system has been presented. We have so far discussed the general architecture of a multiband OFDM sounding system. Subsequently, a detailed formulation and numerical implementation of the MB-OFDM signal design has been presented, while a low PAPR transmitter waveform was designed for MB-OFDM sounding, whose PAPR results were validated. Using the proposed sounding architecture and probing signal, a high-resolution CIR performance has been validated by comparing results from known CIR, LS, LS-DFT, and FPTC, the results of which in turn validate that a high-resolution impulse response can indeed be obtained through the broadband sounding technique proposed herein. Accordingly, the proposed flexible architecture has the capability to allow a vast range of use cases beyond channel sounding, such as those in radar sensing. Nevertheless, there are still gaps in the channel estimation techniques for a sounding application that will be further explored in a future work.

Author's Contributions

Conceptualization, AI, VJ. Funding acquisition, GS, MS. Investigation and methodology, AI, VJ, NZ. Supervision, MD, AAA, VJ. Writing of the original draft, AI. Writing of the review and editing, VJ, MD, AAA, NZ, GS, MS. Formal analysis, AI.

Funding

This study has received funding for publication from the European Union's Horizon 2020 research & innovation programme under grant agreement No. 854194.

Competing Interests

The authors declare that they have no competing interests.

References

[1] Z. Yang, K. Qian, C. Wu, and Y. Zhang, "Passive human detection with Wi-Fi," in *Smart Wireless Sensing*. Singapore: Springer, 2021, pp. 25-45. https://doi.org/10.1007/978-981-16-5658-3_3

[2] A. Czyzewski, J. Kotus, and G. Szwoch, "Estimating traffic intensity employing passive acoustic radar and enhanced microwave Doppler radar sensor," *Remote Sensing*, vol. 12, no. 1, article no. 110, 2020. https://doi.org/10.3390/rs12010110

[3] K. Shi, S. Schellenberger, C. Will, T. Steigleder, F. Michler, J. Fuchs, R. Weigel, C. Ostgathe, and A. Koelpin, “A dataset of radar-recorded heart sounds and vital signs including synchronised reference sensor signals,” *Scientific Data*, vol. 7, article no. 50, 2020. https://doi.org/10.1038/s41597-020-0390-1

[4] Q. Tan, "Processing and manufacturing technology of special sensors," in *Precision Machines*. Singapore: Springer, 2020, pp. 401-403. https://doi.org/10.1007/978-981-13-0381-4_23

[5] A. Ledergerber and R. D’Andrea, "A multi-static radar network with ultra-wideband radio-equipped devices," *Sensors*, vol. 20, no. 6, article no. 1599, 2020. https://doi.org/10.3390/s20061599

[6] M. M. Jatlaoui, P. Pons, and H. Aubert, "Pressure micro-sensor based on radio-frequency transducer," in *Proceedings of IEEE MTT-S International Microwave Symposium Digest*, Atlanta, GA, 2008, pp. 1203-1206.

[7] K. Suresh, V. Jeoti, M. Drieberg, S. Soeung, A. Iqbal, G. M. Stojanovic, and S. Sarang, “Simultaneous detection of multiple surface acoustic wave sensor-tags for water quality monitoring utilizing cellular code-reuse approach,” *IEEE Internet of Things Journal*, 2021. https://doi.org/10.1109/JIOT.2021.3082141

[8] C. Qi, F. Amato, Y. Guo, Y. Zhang, and G. D. Durgin, "A backscatter channel sounder using tunneling RFID tags," in *Proceedings of 2021 IEEE International Conference on RFID (RFID)*, Atlanta, GA, 2021, pp. 1-7.

[9] M. W. Akhtar, S. A. Hassan, R. Ghaffar, H. Jung, S. Garg, and M. S. Hossain, "The shift to 6G communications: vision and requirements," *Human-centric Computing and Information Sciences*, vol. 10, article no. 53, 2020. https://doi.org/10.1186/s13673-020-00258-2

[10] C. X. Wang, J. Huang, H. Wang, X. Gao, X. You, and Y. Hao, "6G wireless channel measurements and models: trends and challenges," *IEEE Vehicular Technology Magazine*, vol. 15, no. 4, pp. 22-32, 2020.

[11] E. Vilar and P. A. Matthews, "Measurement of phase fluctuations on millimetric radiowave propagation," *Electronics Letters*, vol. 7, no. 18, pp. 566-568, 1971.

[12] J. D. Parsons, D. A. Demery, and A. M. D. Turkmani, "Sounding techniques for wideband mobile radio channels. A review," *IEE Proceedings, Part I: Communications, Speech and Vision*, vol. 138, no. 5, pp. 437-446, 1991.

[13] R. J. Pirkl and G. D. Durgin, "Optimal sliding correlator channel sounder design," *IEEE Transactions on Wireless Communications*, vol. 7, no. 9, pp. 3488-3497, 2008.

[14] A. G. Siamarou, "A swept-frequency wideband channel sounding system at the 63.4-64.4 GHz Band with 1 ns time-resolution," *International Journal of Infrared and Millimeter Waves*, vol. 29, no. 12, pp. 1186-1195, 2008.

[15] I. Sfar, L. Osman, and A. Gharsallah, "Wideband demodulator based on five-port correlator for channel sounding applications," *Journal of Electromagnetic Analysis and Applications*, vol. 5, no. 2, pp. 79-84, 2013.

[16] L. A. Lopez-Valcarcel and M. Garcia Sanchez, "A wideband radio channel sounder for non-stationary channels: design, implementation and testing," *Electronics*, vol. 10, no. 15, article no. 1838, 2021. https://doi.org/10.3390/electronics10151838

[17] V. Dear, A. Purwono, I. Iskandar, A. Kurniawan, and P. Abadi, "Design of sliding correlator channel sounder for ionospheric channel probing based on software define radio," *Buletin Pos dan Telekomunikasi*, vol. 19, no. 1, pp. 1-14, 2021.

[18] D. Shakya, T. Wu, and T. S. Rappaport, "A wideband sliding correlator based channel sounder in 65 nm CMOS: an evaluation board design," in *Proceedings of 2020 IEEE Global Communications Conference (GLOBECOM)*, Taipei, Taiwan, 2020, pp. 1-6.

[19] M. Schmieder, W. Keusgen, M. Peter, S. Wittig, T. Merkle, S. Wagner, M. Kuri, and T. Eichler, “THz channel sounding: design and validation of a high performance channel sounder at 300 GHz,” in *Proceedings of 2020 IEEE Wireless Communications and Networking Conference Workshops (WCNCW)*, Seoul, Korea, 2020, pp. 1-6.

[20] G. Korzeniewski and R. C. Alvarez, "Industrial wireless channel measurements in a 2.4 GHz ISM radio band using a low-cost SDR-based channel sounder," *ReCIBE, Revista electrónica de Computación, Informática, Biomédica y Electrónica*, vol. 9, no. 1, pp. E1-25, 2020.

[21] M. Anderson, G. Borg, and R. Goodwin, "Channel sounding measurements at 59.5 MHz across the Australian capital territory," in *Proceedings of 2005 Asia-Pacific Conference on Communications*, Perth, Australia, 2005, pp. 705-709.

[22] R. J. Pirkl, "A sliding correlator channel sounder for ultra-wideband measurements," M.S. thesis, Georgia Institute of Technology, Atlanta, GA, 2007.

[23] K. Sarabandi, N. Behdad, A. Nashashibi, M. Casciato, L. Pierce, and F. Wang, "A measurement system for ultrawide-band communication channel characterization," *IEEE Transactions on Antennas and Propagation*, vol. 53, no. 7, pp. 2146-2155, 2005.

[24] Y. Lyu, A. W. Mbugua, K. Olesen, P. Kyosti, and W. Fan, "Design and validation of the phase-compensated long-range sub-THz VNA-based channel sounder," *IEEE Antennas and Wireless Propagation Letters*, vol. 20, no. 12, pp. 2461-2465, 2021.

[25] H. A. Taleb, K. Ghanem, M. Z. Zaaimia, I. B. Mabrouk, and M. Nedil, "On 60 GHz MIMO diversity in an underground mine propagation channel," *IEEE Antennas and Wireless Propagation Letters*, vol. 19, no. 10, pp. 1769-1773, 2020.

[26] X. Cai, G. Zhang, C. Zhang, W. Fan, J. Li, and G. F. Pedersen, "Dynamic channel modeling for indoor millimeter-wave propagation channels based on measurements," *IEEE Transactions on Communications*, vol. 68, no. 9, pp. 5878-5891, 2020.

[27] C. Y. Yehl, C. P. Lail, M. C. Tseng, and H. J. Li, "An OFDM-based channel sounder system," in *Proceedings of 2009 IEEE Antennas and Propagation Society International Symposium*, 2009, North Charleston, SC, pp. 1-4.

[28] J. K. Hwang, K. H. Lin, Y. L. Chiu, and J. D. Li, "An OFDM-based multipath channel sounding method with fractional delays resolution," in *Proceedings of 2010 IEEE International Conference on Wireless Information Technology and Systems*, Honolulu, HI, 2010, pp. 1-4.

[29] H. S. Kim, S. H. Lee, and Y. H. Lee, "Channel sounding for multi-sector cooperation in OFDM-based wireless cellular systems," in *Proceedings of the 12th International Conference on Advanced Communication Technology (ICACT)*, Gangwon, Korea, 2010, pp. 313-317.

[30] D. Sugizaki, N. Iwakiri, and T. Kobayashi, "Ultra-wideband spatio-temporal channel sounding with use of an OFDM signal in the presence of narrowband interference," in *Proceedings of 2010 4th International Conference on Signal Processing and Communication Systems*, Gold Coast, Australia, 2010, pp. 1-10.

[31] R. M. L. Silva, G. L. Siqueira, L. H. Gonsioroski, and C. R. V. Ron, "Comparison between OFDM and STDCC mobile channel sounders at 3.5 GHz," *Journal of Microwaves, Optoelectronics and Electromagnetic Applications*, vol. 12, no. 1, pp. 1-14, 2013.

[32] O. Seijo, I. Val, and J. A. Lopez-Fernandez, "Portable full channel sounder for industrial wireless applications with mobility by using sub-nanosecond wireless time synchronization," *IEEE Access*, vol. 8, pp. 175576-175588, 2020.

[33] O. Seijo, I. Val, and J. A. Lopez-Fernandez, "Portable full channel sounder for mobile robotics by using sub-nanosecond time synchronization over wireless," in *Proceedings of 2020 16th IEEE International Conference on Factory Communication Systems (WFCS)*, Porto, Portugal, 2020, pp. 1-4.

[34] M. B. Khalilsarai, B. Gross, S. Stefanatos, G. Wunder, and G. Caire, "WiFi-based channel impulse response estimation and localization via multi-band splicing," in *Proceedings of 2020 IEEE Global Communications Conference (GLOBECOM)*, Taipei, Taiwan, 2020, pp. 1-6.

[35] T. Kazaz, G. J. M. Janssen, J. Romme, and A. J. V. d. Veen, "Delay estimation for ranging and localization using multiband channel state information," *IEEE Transactions on Wireless Communications*, vol. 21, no. 4, pp. 2591-2607, 2022.

[36] T. Zwick, T. J. Beukema, and H. Nam, "Wideband channel sounder with measurements and model for the 60 GHz indoor radio channel," *IEEE Transactions on Vehicular Technology*, vol. 54, no. 4, pp. 1266-1277, 2005.

[37] C. U. Bas, V. Kristem, R. Wang, and A. F. Molisch, "Real-time ultra-wideband frequency sweeping channel sounder for 3–18 GHz," in *Proceedings of 2017 IEEE Military Communications Conference (MILCOM)*, Baltimore, MD, 2017, pp. 775-781.

[38] T. Srisooksai, J. I. Takada, and K. Saito, "Portable wide-band channel sounder based software defined radio for studying the radio propagation in an outdoor environment," in *Proceedings of 2017 International Symposium on Antennas and Propagation (ISAP)*, Phuket, Thailand, 2017, pp. 1-2.

[39] E. Blossom, "GNU radio: tools for exploring the radio frequency spectrum," *Linux Journal*, vol. 2004, no. 122, article no. 4, 2004.

[40] J. Li, Y. Zhao, C. Tao, and B. Ai, "System design and calibration for wideband channel sounding with multiple frequency bands," *IEEE Access*, vol. 5, pp. 781-793, 2017.

[41] M. S. Amjad, G. S. Pannu, A. Memedi, M. Nabeel, J. Blobel, F. Missbrenner, and F. Dressler, "A flexible real-time software-based multi-band channel sounder," in *Proceedings of 2020 IEEE 31st Annual International Symposium on Personal, Indoor and Mobile Radio Communications*, London, UK, 2020, pp. 1-6.

[42] Y. Rahmatallah and S. Mohan, "Peak-to-average power ratio reduction in OFDM systems: a survey and taxonomy," *IEEE Communications Surveys & Tutorials*, vol. 15, no. 4, pp. 1567-1592, 2013.

[43] R. Yang and R. S. Sherratt, "Multiband OFDM modulation and demodulation for ultra wideband communications," in *Novel applications of the UWB Technologies*. Rijeka, Croatia: InTech, 2011, pp. 3-30.

[44] W. P. Siriwongpairat and K. J. Ray Liu, *Ultra-Wideband Communications Systems: Multiband OFDM Approach*. Hoboken, NJ: John Wiley & Sons, 2007.

[45] T. Newton, "Channel sounding in white space spectrum, application notes, Rohde & Schwarz," 2011 [Online]. Available: http://www.rohde-schwarz.com/en/applications/channel-sounding-in-white-space-spectrum-application-note_56280-15762.html.

[46] I. Baig and V. Jeoti, "PAPR reduction in OFDM systems: Zadoff-Chu matrix transform based pre/post-coding techniques," in *Proceedings of 2010 2nd International Conference on Computational Intelligence, Communication Systems and Networks*, Liverpool, UK, 2010, pp. 373-377.

[47] A. Iqbal, V. Jeoti, M. Drieberg, and W. P. Wen, "Chu sequence based phasing scheme for low PAPR multicarrier waveform for channel sounding," in *Proceedings of 2017 IEEE 30th Canadian Conference on Electrical and Computer Engineering (CCECE)*, Windsor, Canada, 2017, pp. 1-4.

[48] R. K. Mohammed, "Comparing various channel estimation techniques for OFDM systems using MATLAB," *International Journal of Wireless & Mobile Networks (IJWMN)*, vol. 11, no. 3, pp. 19-31, 2019.

[49] A. M. Khan, V. Jeoti, and M. A. Zakariya, "Improved pilot-based LS and MMSE channel estimation using DFT for DVB-T OFDM systems," in *Proceedings of 2013 IEEE Symposium on Wireless Technology and Applications (ISWTA)*, Kuching, Malaysia, 2013, pp. 120-124.

[50] Y. Wang, G. Zhang, Z. Xie, and J. Hu, "Channel estimation in DCT-based OFDM," *The Scientific World Journal*, vol. 2014, article no. 813429, 2014. https://doi.org/10.1155/2014/813429

[51] J. Haifang and S. Yin, "An efficient iterative DFT-based channel estimation for MIMO-OFDM systems on multipath channels," in *Proceedings of 2008 3rd International Conference on Communications and Networking in China (ChinaCom)*, Hangzhou, China, 2008, pp. 45-49.

[52] A. M. Khan, V. Jeoti, M. Z. U. Rehman, M. T. Jilani, and M. A. Zakariya, "A cyclic correlation-based time domain channel estimation scheme," in *Proceedings of 2016 6th International Conference on Intelligent and Advanced Systems (ICIAS)*, Kuala Lumpur, Malaysia, 2016, pp. 1-5.

[53] M. Morelli and U. Mengali, "A comparison of pilot-aided channel estimation methods for OFDM systems," *IEEE Transactions on Signal Processing*, vol. 49, no. 12, pp. 3065-3073, 2001.